JACS
JOURNAL OF THE AMERICAN CHEMICAL SOCIETY

Article

pubs.acs.org/JACS

Photonic Crystal Microbubbles as Suspension Barcodes

Luoran Shang,[†,§] Fanfan Fu,[†,§] Yao Cheng,[†] Huan Wang,[†] Yuxiao Liu,[†] Yuanjin Zhao,*[,†,‡] and Zhongze Gu*[,†,‡]

[†]State Key Laboratory of Bioelectronics, School of Biological Science and Medical Engineering, Southeast University, Nanjing 210096, China

[‡]Laboratory of Environment and Biosafety, Research Institute of Southeast University in Suzhou, Suzhou 215123, China

Supporting Information

ABSTRACT: A novel suspension array was developed that uses photonic crystal (PhC) microbubbles as barcode particles. The PhC microbubbles have an outer transparent polymeric shell, a middle PhC shell, and an inner bubble core, and they were achieved by extraction-derived self-assembly of colloidal nanoparticles in semipermeable solid microcapsules. The encoded elements of the microbubbles originated from their PhC structure with a coated shell, which not only improved the stability of the codes but also provided a flexible surface for bioassays. By using multicompartmental microcapsule templates, PhC microbubbles with substantial coding levels and controllable movement could also be achieved. In addition, as the size of the encapsulated bubbles could be tailored, the overall density of the PhC microbubbles could be adjusted to match the density of a detection solution and to remain in suspension. These remarkable properties make the PhC microbubbles excellent barcode particles.

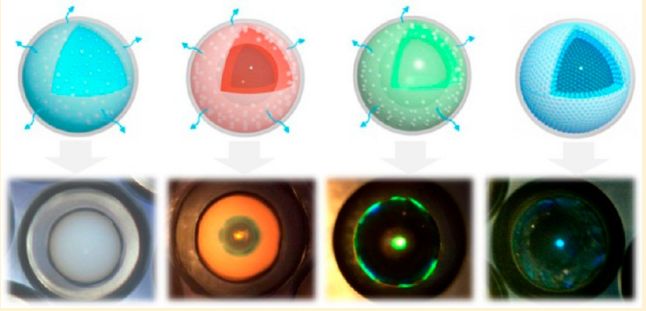

INTRODUCTION

Suspension arrays in which barcode particles are used as elements have a demonstrated value for multiplexed high-throughput bioassays, such as clinical diagnostics and drug discovery.[1−9] Compared with conventional planar arrays, these barcode-particle-based suspension arrays show high flexibility, fast reaction, good reproducibility, and high sensitivity for detection.[4−17] Many encoding strategies have been proposed for these barcode particles, including incorporation of fluorescent molecules,[7−9] quantum dots,[10−12] shapes,[13] patterning,[14,15] and photonic crystals (PhCs).[16−18] Among them, PhCs hold immense promise as barcode elements because of their excellent optical properties, such as minimal spectral width, remarkable stability, and freedom from fluorescent background.[19−26] However, because of the high density of the polymer materials, current barcode particles, including PhC particles, actually deposit rapidly rather than remain in suspension in the reaction mixture. This would reduce the radial diffusion efficiency of the barcode particles and thus greatly depress their detection efficiency. In addition, the possible code number of the simple PhC particles is limited in practical terms by the availability of reflection peaks with distinct identification. These defects, together with uncontrollable motion and inefficient surface activity, have greatly restricted the practical application of these particles. Therefore, the creation of new barcode particles with distinct advantages is still anticipated.

In this paper, we present a new type of barcode particle with the desired functions. The particles were derived from microfluidic solid microcapsules with a semipermeable membrane shell and a colloidal-nanoparticle-encapsulated liquid core. By dispersing the microcapsules in an ethanol solution to extract water from the core, their encapsulated colloidal nanoparticles could be gradually concentrated and self-assembled into the hollow spherical PhC shell on the inner wall of the microcapsules, as schematically shown in Figure 1. The resultant PhC microbubbles were composed of an outer transparent polymeric shell, a middle PhC shell, and an inner bubble core, and they were employed as barcode particles. The encoded elements of the particles originated from their PhC structure with a coated shell, which not only improved the stability of the codes but also provided a flexible surface for bioassays. In addition, by using multicompartmental PhC microbubbles, the barcode particles allow for a substantial number of coding levels and for controllable movement in multiplexing applications. More importantly, as the size of the encapsulated core and the corresponding bubbles of the barcode particles could be tailored in their emulsification process, the overall density of the PhC microbubbles could be adjusted to match the density of a detection solution so that they remain in suspension. These features make the PhC

Received: October 10, 2015
Published: December 1, 2015

DOI: 10.1021/jacs.5b10612
J. Am. Chem. Soc. 2015, 137, 15533−15539

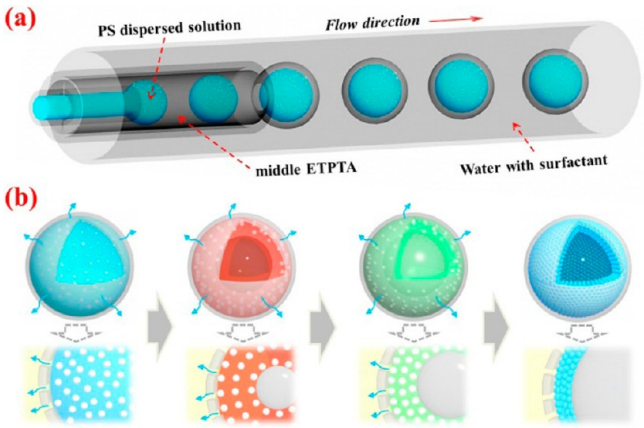

Figure 1. Schematic illustration of the (a) microfluidic emulsification process and (b) concentration and self-assembly of water-extraction-derived colloidal nanoparticles into a hollow spherical PhC shell on the inner wall of the microcapsules.

microbubbles excellent functional barcode particles in biomedical applications.

EXPERIMENTAL SECTION

Materials. Aqueous surfactants ethylene oxide−propylene oxide−ethylene oxide triblock copolymer (Pluronic F108), poly(vinyl alcohol) (PVA), photocurable ethoxylated trimethylolpropane triacrylate (ETPTA) resin, photoinitiator 2-hydroxy-2-methylphenylpropanone (HMPP), hydrophobic reagent octadecyltrichlorosilane (OTS), and fluorescent polystyrene nanoparticles (for CLSM characterization only) were all derived from Sigma-Aldrich Co. The ultrafine Fe_2O_3 nanoparticles (50 nm mean diameter) were obtained from Jiangsu Laboratory for Biomaterials and Devices. Monodisperse charged polystyrene (PS) nanoparticles (with diameters of 190, 205, 215, 230, 240, 270, and 290 nm, respectively) were purchased from Nanjing Dongjian Biological Technology Co., Ltd. (Nanjing, China). Immunoglobulin G (IgG) protein molecules; rabbit, goat, human IgG; and fluorescein isothiocyanate (FITC)-tagged anti-human IgG were purchased from Beijing Biosynthesis Biotechnology Co., Ltd. (Beijing, China). Human hepatoma cells HepG2 were gained from Gulou Hospital, Nanjing. Calcein AM was purchased from Molecular Probes. Ethanol and NaOH (AR) were gained from Sinopharm Chemical Reagent Co., Ltd. (Shanghai, China). Bovine serum albumin (BSA) and phosphate-buffered saline (PBS) were all self-prepared. Deionized water was used in all experiments.

Microfluidic Chip Construction. The microfluidic device was constructed by assembling glass capillaries on a glass slide. The inner, middle, and outer cylindrical capillaries were identical and all gained from World Precision Instruments, Inc. The inner and outer diameters of the capillaries were 580 μm and 1 mm, respectively. The square capillary with an inner diameter of 1.05 mm was purchased from VitroCom, Inc. The inner capillary was tapered using a laboratory portable Bunsen burner (Honest MicroTorch). The capillary was stretched by hand to reach a diameter of about 80 μm at the orifice. The middle capillary was tapered by a micropipet puller (Sutter Instrument Co.) and was sanded under an optical microscope to reach the desired orifice diameter of about 300 μm. For the treatment of the middle capillary, the inner wall was wetted by the hydrophobic reagent OTS and incubated for 30 min. After this, the solution was blown out by nitrogen. Then the three capillaries were coaxially and sequentially assembled on a glass slide. To integrate fluids conveniently and to observe the emulsification process, the square capillary was added around the contact area of the middle and outer capillary. The connectors of the assembled capillaries were sealed with dispensing needles and transparent epoxy resin (Devcon 5 Minute Epoxy) where necessary.

Photonic Crystal Microbubbles Generation. The inner and middle phases flowed through the inner and middle capillary, respectively, in the same direction. The continuous phase flowed via the interstices between the square capillary and the middle capillary or between the square capillary and the outer capillary. The inner phase was an aqueous solution of surfactant F108 (2 wt %) with PS nanoparticles (10 wt %). The middle oil phase was a photocurable ETPTA resin with 1% photoinitiator. The outer phase was a mixture of two surfactant solutions (2 wt % F108 and 10 wt % PVA, with volume ratio of 2:1). Each fluid was pumped by a syringe pump (Harvard PHD 2000 Series) and was connected through a polyethylene tube (Scientific Commodities Inc., with inner and outer diameters of 0.86 and 1.32 mm, respectively) with a glass syringe (SGE Analytical Science). The three phases were induced to the microfluidic device in a sequential coflow regime, and double emulsions were generated in the outer capillary. The production rate was controlled by adjusting flow rates, ranging from several to dozens of droplets per second. For multicore emulsions generation, the same device was applied, and flow rates of the three phases were adjusted. In our case, the flow rate of the inner phase was comparative to or slightly higher than that of the middle phase to achieve simultaneous encapsulation of more than one core drop within the shell. A typical set of the inner, middle, and outer flow rates were 0.5, 0.5, and 3 mL/h for double-core emulsions and 0.5, 0.35, and 3 mL/h for triple-core emulsions, respectively. The droplets were solidified downstream upon in situ UV irradiation for 3 s by a UV-light (EXFO OmniCure SERIES 1000, 365 nm, 100 W). To induce surface modification of colloidal silica arrays, the middle oil phase was silica nanoparticles (100 nm diameter) dispersed in ETPTA resin (1 mg/mL). For preparing the silica dispersed in ETPTA solution, silica nanoparticles and ETPTA was first mixed in ethanol. The photoinitiator was then added, with a volume fraction of 1% (V_{HMPP}/V_{ETPTA}). The mixture was placed in an oven to promote complete volatilization of the ethanol. For the generation of multicompartmental microcapsules, distinct inner capillaries need to be incorporated in the microfluidic device. All of the microcapsule templates were immersed in ethanol solution at room temperature for several hours with gentle stirring using a magnetic rotator to extract water and generate the corresponding PhC microbubbles. The as-prepared hollow microparticles were taken out from ethanol solution and dried naturally before they were dispersed in water, the water did not refill when they were resubmerged in the reaction liquid because the internal and external pressure reached equilibrium.

Characterization. The emulsification process in the collection capillary of the device was observed in real time under an inverted microscope (AE2000, Motic) and was recorded by a charge-coupled device (CCD, S-PRI F1, AOS Technologies AG). The optical images of the microcapsules and microbubbles were observed with a stereomicroscope (NOVEL NTB-3A, Ningbo Yongxin Optics Co., Ltd., China) and were captured by a CCD (Media Cybernetics Evolution MP 5.0 RTV). The capsules' evolution process was monitored under the same stereomicroscope, and images and movies were captured by the same CCD aforementioned. Fluorescence photographs of the microbubbles were taken by a laser scanning confocal microscope (Carl Zeiss, LSM510). The microstructures of ruptured microcapsules were characterized by a scanning electron microscope (SEM, HITACHI, S-3000N). Optical properties of the particles were measured by a fiber-optic spectrometer (Ocean Optics, HR2000-FLG) to detect the reflection spectra.

Multiplex Immunoassays. The PhC microbubbles underwent plasma treatment (Suzhou OPS Plasma Tech-nology Co, LTD, China) for 3 min and were immersed in NaOH solution (0.1m) for 10 min to activate the silanol groups on the surfaces. Then, the particles were transferred into an aqueous solution of APTMS (5 vol %) and reacted for 4 h at room temperature with gentle shaking. Afterward, they were washed with phosphate-buffered saline (PBS; pH 5.7) and went through the Schiff's base reaction with glutaric dialdehyde (2.5 v/v% in PBS, pH 5.7, 4 h). Next, the microparticles were washed again with PBS (pH 7.4) and incubated with rabbit, human, or goat IgG (0.5 mg/mL in PBS, 4 °C, 12 h). After washing with PBS (pH 7.4), the

DOI: 10.1021/jacs.5b10612
J. Am. Chem. Soc. 2015, 137, 15533−15539

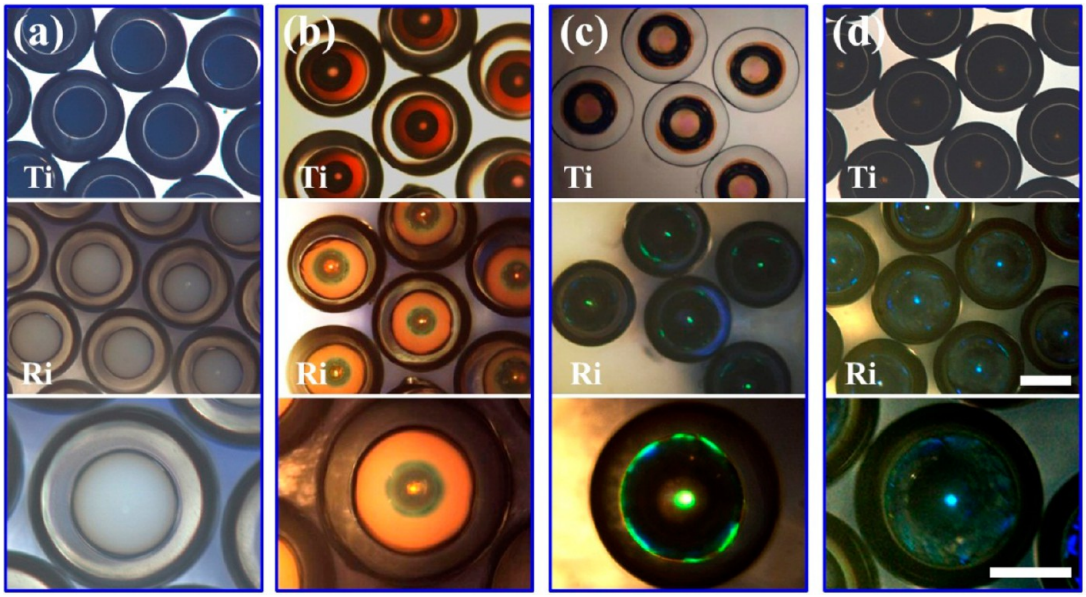

Figure 2. Transmission images (Ti, first row) and the corresponding reflection images (Ri, second and third rows) of the microcapsules: (a) the initial state, which appeared white due to strong scattering from the random PS arrangement, and (b–d) during the bubble generation and enlargement process, which showed structural color and for which the color blue-shifted gradually. The images in the third row are the enlarged images of the second row. The scale bars are 300 μm.

microspheres were treated with BSA (1% in PBS, room temperature, 2 h) and washed with PBS several times. Finally, FITC-tagged anti-human IgG (20 mg/mL in PBS) was added to the PhC microbubbles mixture and the system was incubated at 31 °C for 3 h. The resulting mixtures were washed with PBST (0.05% Tween-20 in PBS) and water many times. In situ bright-field and fluorescence images were taken by the same aforementioned stereomicroscope in reflection mode, using different filters and light sources.

HepG2 Cell Culture. The PhC microbubbles were immersed in 75% ethanol solution for 8–12 h and washed by sterile PBS solution before being irradiated with ultraviolet light for disinfection before cell culture. Then we transferred the microcarriers to a 96-well plate. After this, an appropriate amount of HepG2 suspension (2×10^6 cells/mL) was added to the plate to allow the attachment of cells to the surface of microspheres. A universal shaker was employed to increase the contact opportunity between cells and the PhC microbubbles before forming focal adhesion. The microcarriers were placed in the incubator for 24 h (37 °C; 5% CO_2). In general, the cell-loaded PhC microbubbles would be used for further research after another 1 or 2 days of culture. Fluorescence staining was applied to detect the cell viability of HepG2 cells. Briefly, the HepG2-cell-loaded PhC microbubbles were incubated with Calcein-AM solution (10 μM, 20 min, room temperature) and fixed with glutaraldehyde solution (2.5%, 30 min, room temperature). Finally, they were stored in PBS, and the in situ bright-field and fluorescence images were taken by the same aforementioned stereomicroscope in reflection mode, using different filters and light sources. In order to characterize the cell morphology, the cell-loaded PhC microbubbles were washed repeatedly and dehydrated with a gradient of ethanol before SEM images were taken.

RESULTS AND DISCUSSION

Microcapsule templates were generated by using a capillary microfluidic double-emulsion device to integrate the inner, middle, and outer fluid phases in a sequential coflow regime, as shown in Figure 1a and Figure S1 [Supporting Information (SI)]. Because of the advantages in controlling the structures of the emulsion, microfluidic techniques have emerged as a versatile method for generating monodisperse emulsion droplets with complicated structures.[27−29] The emulsion droplets have been applied as templates to fabricate functional particles for different applications.[30−38] Here, an immiscible aqueous phase of monodisperse charged PS nanoparticles and an oil phase of ETPTA were used as the inner and middle fluids, and thus, after photopolymerizing the microfluidic emulsified double-emulsion droplets, solid monodisperse ETPTA microcapsules were obtained (Figure S1b,d,f, SI), with a colloidal liquid core containing nanoparticles. This stepwise microfluidic strategy has proven to be superior to bulk emulsification strategies, and has enabled precise fabrication of one drop at a time and, thus, ensured high monodispersity of the resultant microcapsules. In addition, by adjusting the flow rates of the flow streams, the size and the core numbers of the microcapsules could be readily adjusted (Figure S1, SI).

The as-prepared microcapsules were then immersed in ethanol, which served as a water-absorbing agent. Because of the selective permeability of the highly cross-linked ETPTA polymer,[39] the water in the core of the microcapsules could be drawn out across the shell, whereas the PS nanoparticles were protected from extravasation and the ethanol was prevented to enter the core. When the liquid pressure decreased to a critical level, a bubble instantly emerged within the core to relax the tension. The evidence of the bubble formation was confirmed by artificially puncturing the microcapsule and releasing it, as recorded in Movie S1 (SI). The mechanism of the bubble formation is a typical cavitation phenomenon, in which vapor bubbles form spontaneously by aggregating submerged small gas nuclei to relatively large volumes when the pressure acting on a liquid is decreased beyond a critical tension.[40−42] It should be noted that the ETPTA shell should be thicker than 20 μm to avoid the rupture of the microcapsules during the ethanol treatment.

The entrapped bubble then expanded steadily over time and the concentration of the PS colloidal nanoparticles in the remaining water increased. During this process, the PS nanoparticles adsorb at the solid–liquid interface to minimize total interfacial energy[43] and gradually assemble in the confined inner wall of the microcapsules. This process is shown in Figure

DOI: 10.1021/jacs.5b10612
J. Am. Chem. Soc. 2015, 137, 15533−15539

2. It can be observed that the microcapsules appeared white at the beginning because of strong scattering from the random PS arrangement (Figure 2a). With the continuous outward flux of water, the PS nanoparticles concentrated and the spacing between nanoparticles reduced gradually.

When the concentration increased to a certain degree, significant interparticle repulsion occurred and the nanoparticles assembled into a non-close-packed colloidal crystal array structure owing to the minimum energy configuration. The periodic arrangement of the colloidal particles would give rise to a photonic band gap in the PS suspension. Light of a certain wavelength located in this band gap was prohibited from propagating and thus could be reflected. Thus, the suspension appeared to be of iridescent color and possessed a characteristic reflection peak. The main reflection peak position λ can be estimated by Bragg's equation for a normal incident beam onto the (111) plane of the face-centered-cubic (fcc) structure

$$\lambda = 1.633 d n_{av} \quad (1)$$

where d is the center-to-center distance between two adjacent nanoparticles and n_{av} is the average refractive index of the hybrid PS suspension. Therefore, the concentration process resulted in the decrease of d and the corresponding λ, which caused the blue-shift of the structural color (Figure 2b,c). When the water in the liquid core of the microcapsules was completely pumped out, the PS nanoparticles assembled into a stably close-packed pattern and formed PhC microbubbles (Figure 2d). Distinct from the classical bottom-up 3D assembly patterns, where colloidal nanoparticles assemble in bulk or at planar or curved surfaces to form films, we put forward this novel type of assembly at a spherical surface and achieved uniformly hollow colloidal PhC shells. To our knowledge, this has never been reported previously. These hollow PhC microbubbles should have important value in the construction of efficient microwave antennas, low-loss resonators, zero-threshold lasers or microlasers, sensors, etc.

As the hydrosoluble PS nanoparticles could only stay in the residual water of the cores during the process of the extraction-derived colloidal assembly, they formed a uniform solid colloidal crystal layer on the inner surface of the microcapsule shell with complete drawing-out of the water from the cores, as observed by a confocal microscope in Figure S2 (SI). This phenomenon could be ascribed to the omnibearing water extraction across the ETPTA shells during the treatment. To further confirm this effect, the microstructure of the resultant PhC bubble was investigated by scanning electron microscopy (SEM), as shown in Figure 3. As can be seen from the cross-sectional view of a microcapsule after being cut, the PS nanoparticles formed a uniform solid layer at the inner wall of the PhC bubble ETPTA shell (Figure 3b, depicted by a yellow arrow). The magnified view of the solid PS layer showed that the nanoparticles assembled into a hexagonal close-packed colloidal crystal array structure (Figure 3c,d), which was consistent with the origin of the structural color of the microcapsules. It is worth noting that it was difficult to achieve the structure of the uniformly hollow colloidal PhC shells (PhC microbubbles) in other ways, such as drying and evaporating the core water. This difficulty was attributed to the asymmetrical solvent evaporation or to the low adhesion of the ETPTA inner surface (Figure S3, SI).

The PhC microbubbles were hollow spheres composed of a solid shell and a gas core; thus, the volume ratio of the gaseous to solid part determined their overall density. Tracing back to the generation principle of these PhC microbubbles in microfluidics, this volume ratio could be controlled by changing the flow rates of inner (F_i) and middle (F_m) fluid phases in the emulsification process. Specifically, the density of these PhC microbubbles (ρ) could be calculated as follows:

$$\rho = (F_i\omega + F_m\rho_E)/(F_i + F_m) \quad (2)$$

where ρ_E represents the density of ETPTA and ω is the mass volume fraction of the PS nanoparticles in the colloidal suspension (the detailed derivation of this equation is provided in the SI). To confirm this law, we chose water as a density test reagent and let ρ be equal to 1 g/mL. Typically, ρ_E = 1.12 g/mL and ω was 10 wt %. Thus, the functional relationship between F_i and F_m was deduced as

$$F_m = 7.5F_i \quad (3)$$

According to eq 3, we generated PS-nanoparticle-encapsulated microcapsules and the corresponding PhC microbubbles. Next, they were each dispersed in water. It was found that the liquid-filled microcapsule templates deposited rapidly to the bottom of a vial (i in Figure 4b), while the PhC microbubbles with vivid blue color remained suspended for a long time (ii and iii in Figure 4b). We also drew two theoretical curves about the relationship between F_i and F_m with variations of ω, and the experimental data were consistent with these calculations (Figure S4, SI). It was thus speculated that through simple adjustment of the flow rates, the overall density of the PhC microbubbles could be predetermined to match that of a certain detection solution. This density-tunable feature of PhC microbubbles is highly desired for barcode-particle-based suspension arrays.

Another distinctive feature of the PhC microbubbles was their stable and substantial number of coding levels. In this system, the structural colors or reflection peaks of the PhC layer could be used as encoded elements, and the outer transparent ETPTA shell did not block the coding. Instead, it protected the PhC structure from external disturbances and thus improved coding stability. As can be deduced in eq 1, by varying the diameter of the PS nanoparticles, a series of PhCs

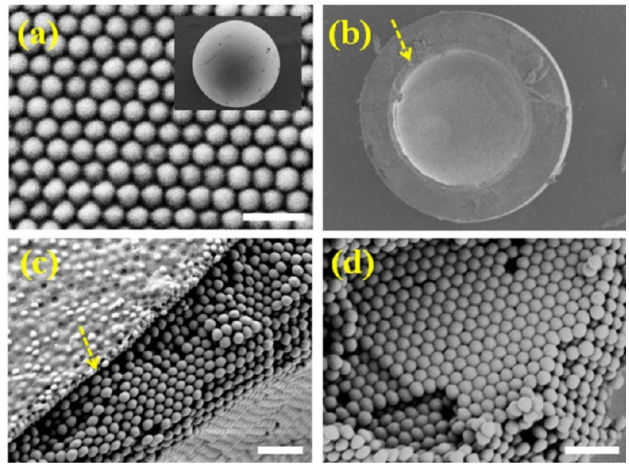

Figure 3. Scanning electron microscopy (SEM) images of the PhC microbubble: (a) microbubble surface decorated with the silica nanoparticles, (b) a cross-sectional image of a microbubble showing the dual shell structure, (c, d) the magnified images of the colloidal crystal layer at the cross-section and bottom of the microbubble. The scale bars are 100 μm in panel a and 1 μm in panels c and d.

DOI: 10.1021/jacs.5b10612
J. Am. Chem. Soc. 2015, 137, 15533−15539

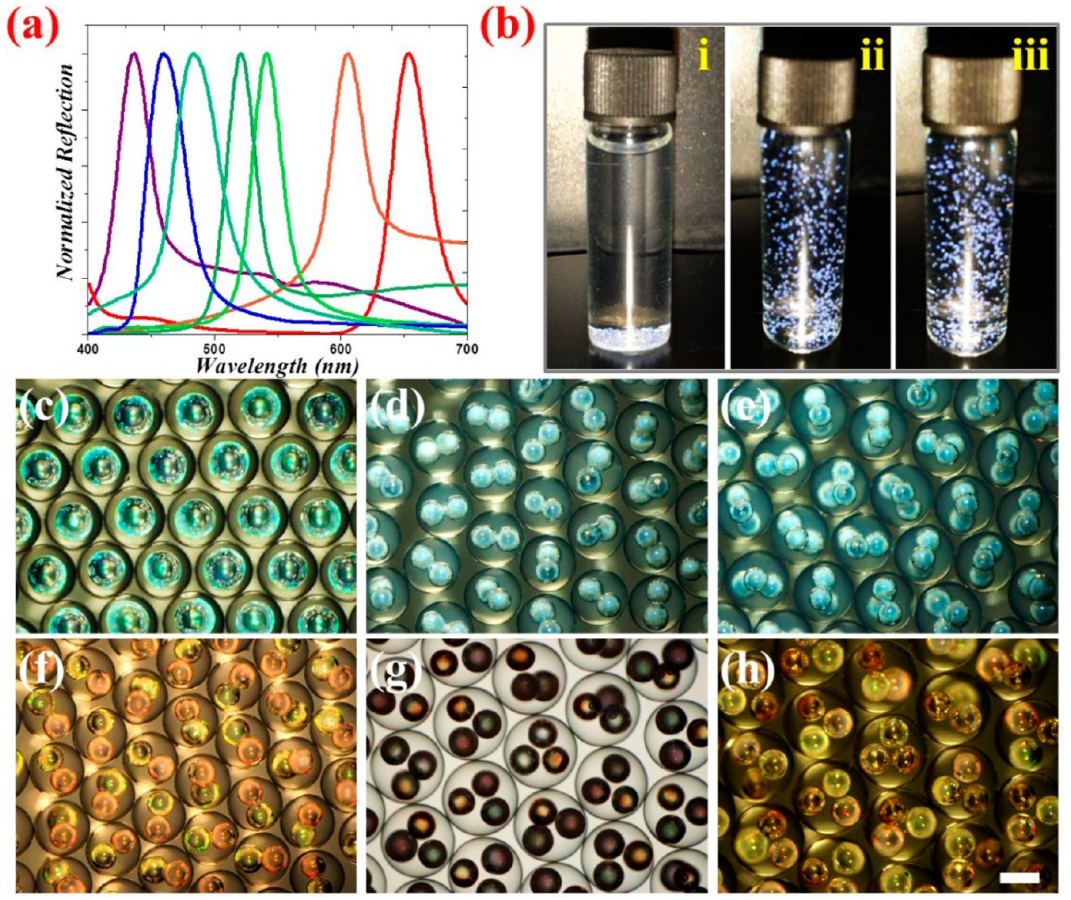

Figure 4. (a) Reflection spectra of the different PhC bubbles. The vertical axis value represents the normalized reflection intensity, and each curve was measured using a single PhC bubble. Due to the quality variation of the nanoparticles, the reflection intensities were not uniform. From left to right, the sizes of the PS nanoparticles are 190, 205, 215, 230, 240, 270, and 290 nm, respectively. (b) Suspending property of the PhC bubbles. The liquid-filled microcapsule templates sank to the bottom of a vial (i), while the gas-filled PhC bubbles could remain in suspension for a long time (ii, iii). (c–e) Microscope photographs of PhC bubbles with different amounts of blue cores. (f–h) Microscope photographs of PhC bubbles with two different cores (f) and three different cores (g, h); panels g and h are the transmission and reflection images, respectively. The scale bar is 300 μm.

with different reflection peak positions and colors could be obtained (Figure 4a). In addition, the PhC microbubbles were endowed with multiple functions through the fabrication of a series of multicompartmental PhC microbubbles by using colloidal suspensions of PS nanoparticles with different diameters as separate inner phases in microfluidics (Figure S5, SI). As the liquid cores were separated by solid ETPTA, each of them served as a discrete niche for water extraction and colloidal assembling without interference. Thus, multcompartmental PhC microbubbles with different color combinations were obtained, as presented in Figure 4f and Figure S6 (SI). The total achievable combinations could increase dramatically with the number of cores and structural color elements. Therefore, the PhC microbubbles allow for a remarkable coding capacity for multiplexing applications.

To impart the PhC microbubbles with additional functions, such as magnetically controllable motion, an aqueous suspension of ultrafine Fe_2O_3 nanoparticles was introduced as one of the inner phases, along with the other inner phases of colloidal suspensions. During extraction-derived assembly, the magnetic Fe_2O_3 nanoparticles eventually formed a uniform spherical solid crystal layer. Thus, multicompartmental magnetoresponsive PhC microbubbles were generated, as shown in Figure 4g,h. Because of the anisotropic distribution of the magnetic niche in the microcapsules, the PhC microbubbles rotate under a rotating magnetic field and can be pulled to the side of a vial using a permanent magnet (see Movie S2, SI). This enables simple capture and enrichment of the PhC microbubbles in bioassays. It is worth noting that by using ETPTA with dispersed silica nanoparticles as the middle phase or an aqueous solution with dispersed silica nanoparticles as the outer phase during the emulsification, the derived PhC microbubble surfaces were decorated with colloidal silica arrays (Figure 3a), which provided flexible chemical and structural features for the bimolecular immobilization and reaction.

To demonstrate the various capabilities of our PhC microbubbles in bioassays, we performed a series of proof-of-principle experiments. Typically, three kinds of PhC microbubbles with red, green and blue structural colors were immobilized with three different antibodies (probe 1, probe 2, and probe 3), respectively. Then, they were mixed and incubated in a test tube, which contained only a solution of a particular FITC-tagged biomolecule (called target 1) for immunoassay. The structural colors of these PhC microbubbles remained constant during the application. Because of the specific binding between the probes and their corresponding targets, it was expected that the fluorescence signals would be observed only on the barcode particles with the corresponding probes. Our results were consistent with the expectation, as shown in Figure 5a,b, that only PhC microbubbles with

DOI: 10.1021/jacs.5b10612
J. Am. Chem. Soc. 2015, 137, 15533–15539

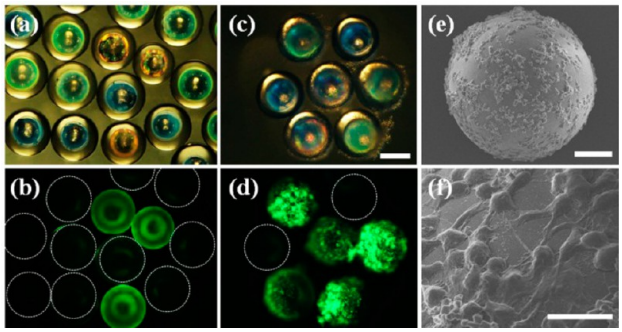

Figure 5. (a, b) Optical and the corresponding fluorescence microscope images of three encoded PhC bubbles after immunoassay. (c, d) Optical and the corresponding fluorescence microscope images of the three encoded PhC bubbles after HepG2 cell culture. (e, f) SEM images showing that the HepG2 cells adhered on the entire spherical surface of the PhC bubbles with a collagen-decorated nanopatterned surface. The scale bars are 300 μm in panels a–d, 100 μm in panel e, and 30 μm in panel f.

antibody probes complementary to the target proteins showed green fluorescence. As the microbubbles were with a solid polymer shell, they were very stable during preservation and application. They did not collapse when drying. In addition, the features of the suspension property, substantial coding levels, and ability to control the motion of the microparticles would facilitate the use of this technology for many practical assays.

In addition to biomolecular detection, these PhC microbubbles could also be used for cell culture. Typically, microcarriers should have a diameter of more than 60 μm for cell research. Superior to traditional barcode particles, which have drawbacks such as small size (several micrometers in diameter), incomprehensible encoding, and debatable biocompatibility for cell research, the PhC microbubbles could overcome these difficulties. Their size can be adjusted from several tens to several hundred micrometers to suit cell dimensions during their microfluidic emulsification (to facilitate manual operation, the PhC microbubbles with diameters of over 300 μm were employed here). The encoding information on the PhC microbubbles is encapsulated by solid shells, and thus they are stable when their surfaces are covered by cells. In addition, different kinds of biomaterials could be incorporated into the surface nanopattern to improve the biocompatibility of the PhC microbubbles. To implement this, PhC microbubbles with blue, red, and green structural colors with a flat ETPTA surface, a silica nanopattern surface, and a collagen-decorated nanopattern surface, respectively, were prepared and mixed for a HepG2 cell culture. Figure 5c,d shows the results of this multiplex evaluation of the interactions of the cells and materials. It can be observed that a large number of HepG2 cells grew on the green PhC microbubbles, and only a small amount grew on the red ones, while there were no observable cells on the blue PhC microbubbles (Figure S7, SI). The different performance of the cell populations on the PhC microbubbles should not only be ascribed to the antiadhesion ETPTA and the biocompatible collagen but also to the surface nanostructure of the PhC microbubbles. In addition to providing more surface area for collagen coating, the colloidal silica array decorated surface of the PhC microbubbles could also provide a nanopatterned platform for cell culture with a stereoscopic three-dimensional (3D) morphology (Figure 5e,f). These results indicate that our PhC microbubbles could be used as a versatile platform for the evaluation of different kinds of biomaterials with a high throughput.

CONCLUSIONS

In conclusion, we have developed a new kind of PhC microbubble barcode particle composed of an outer transparent polymeric shell, a middle PhC shell, and an inner bubble core. These PhC microbubbles were simply generated by extraction-derived self-assembly of colloidal nanoparticles in semipermeable solid microcapsules. The encoded elements of the PhC microbubbles originated from their photonic band gap structure with a coated shell, which not only improved the stability of the codes but also provided a flexible surface for bioassays. It was demonstrated that the PhC microbubbles, with the distinct advantages of substantial coding levels, controllable movement, and adjustable density for suspension, could be achieved by tailoring the structures and compartments of their microcapsule templates. Their applications in multiplex detection and cell cultures reflect the flexibility and versatility of a PhC microbubble-based suspension array. This new type of barcode particle is very promising because it overcomes many restrictions of current suspension array techniques, and it is anticipated that it will open new horizons in biomedicine.

ASSOCIATED CONTENT

Supporting Information

The Supporting Information is available free of charge on the ACS Publications website at DOI: 10.1021/jacs.5b10612.

Detailed discussion of the density tunability of the PhC bubbles, real-time images of microfluidic emulsification, CLSM characterization of the PhC bubbles, assembly of colloidal nanoparticles in the core of the microcapsules through other ways, and additional results of multicompartmental PhC bubbles and cell culture experiments (PDF)

Movie S1, which shows the artificial puncturing of the microparticle and observation of the release of microbubble from the microparticle (the evidence of the existence of the encapsulated bubble)(AVI)

Movie S2, which shows the magnetically controllable motion of PhC bubbles; these particles rotated and were pulled to one side of a disk under the guidance of a magnetic field (AVI)

AUTHOR INFORMATION

Corresponding Authors

*yjzhao@seu.edu.cn

*gu@seu.edu.cn

Author Contributions

§L.S. and F.F. contributed equally to this work.

Notes

The authors declare no competing financial interests.

ACKNOWLEDGMENTS

This work was supported by the National Science Foundation of China (Grant Nos. 21473029, 91227124, and 51522302), the NASF Foundation of China (Grant No. U1530260), the National Science Foundation of Jiangsu (Grant No. BK20140028), the Science and Technology Development Program of Suzhou (Grant No. ZXG2012021), the Research Fund for the Doctoral Program of Higher Education of China

DOI: 10.1021/jacs.5b10612
J. Am. Chem. Soc. 2015, 137, 15533–15539

(20120092130006), and the Program for New Century Excellent Talents in University.

REFERENCES

(1) Leng, Y. K.; Sun, K.; Chen, X. Y.; Li, W. W. *Chem. Soc. Rev.* **2015**, *44*, 5552.
(2) Gu, L. C.; Li, C.; Aach, J.; Hill, D. E.; Vidal, M.; Church, G. M. *Nature* **2014**, *515*, 554.
(3) Zheng, F. Y.; Cheng, Y.; Wang, J.; Lu, J.; Zhang, B.; Zhao, Y. J.; Gu, Z. Z. *Adv. Mater.* **2014**, *26*, 7333.
(4) Kelley, S. O.; Mirkin, C. A.; Walt, D. R.; Ismagilov, R. F.; Toner, M.; Sargent, E. H. *Nat. Nanotechnol.* **2014**, *9*, 969.
(5) Zhao, Y. J.; Shang, L. R.; Cheng, Y.; Gu, Z. Z. *Acc. Chem. Res.* **2014**, *47*, 3632.
(6) Lee, J.; Bisso, P. W.; Srinivas, R. L.; Kim, J. J.; Swiston, A. J.; Doyle, P. S. *Nat. Mater.* **2014**, *13*, 524.
(7) Cunin, F.; Schmedake, T. A.; Link, J. R.; Li, Y. Y.; Koh, J.; Bhatia, S. N.; Sailor, M. J. *Nat. Mater.* **2002**, *1*, 39.
(8) Li, Y. Y.; Kollengode, V. S.; Sailor, M. J. *Adv. Mater.* **2005**, *17*, 1249.
(9) Hou, J.; Zhang, H. C.; Yang, Q.; Li, M. Z.; Song, Y. L.; Jiang, L. *Angew. Chem., Int. Ed.* **2014**, *53*, 5791.
(10) Allen, C. N.; Lequeux, N.; Chassenieux, C.; Tessier, G.; Dubertret, B. *Adv. Mater.* **2007**, *19*, 4420.
(11) Chen, Y.; Dong, P. F.; Xu, J. H.; Luo, G. S. *Langmuir* **2014**, *30*, 8538.
(12) Rauf, S.; Glidle, A.; Cooper, J. M. *Adv. Mater.* **2009**, *21*, 4020.
(13) Lin, C. X.; Jungmann, R.; Leifer, A. M.; Li, C.; Levner, D.; Church, G. M.; Shih, W. M.; Yin, P. *Nat. Chem.* **2012**, *4*, 832.
(14) Ke, Y. G.; Lindsay, S.; Chang, Y.; Liu, Y.; Yan, H. *Science* **2008**, *319*, 180.
(15) Lee, H.; Kim, J.; Kim, H.; Kim, J.; Kwon, S. *Nat. Mater.* **2010**, *9*, 745.
(16) Fenzl, C.; Hirsch, T.; Wolfbeis, O. S. *Angew. Chem., Int. Ed.* **2014**, *53*, 3318.
(17) Ye, B. F.; Ding, H. B.; Cheng, Y.; Gu, H. C.; Zhao, Y. J.; Xie, Z. Y.; Gu, Z. Z. *Adv. Mater.* **2014**, *26*, 3270.
(18) Hou, J.; Zhang, H. C.; Yang, Q.; Li, M. Z.; Jiang, L.; Song, Y. L. *Small* **2015**, *11*, 2738.
(19) von Freymann, G.; Kitaev, V.; Lotsch, B. V.; Ozin, G. A. *Chem. Soc. Rev.* **2013**, *42*, 2528.
(20) Shang, L. R.; Shangguan, F. Q.; Cheng, Y.; Lu, J.; Xie, Z. Y.; Zhao, Y. J.; Gu, Z. Z. *Nanoscale* **2013**, *5*, 9553.
(21) Ge, J. P.; Yin, Y. D. *Angew. Chem., Int. Ed.* **2011**, *50*, 1492.
(22) Burgess, I. B.; Loncar, M.; Aizenberg, J. *J. Mater. Chem. C* **2013**, *1*, 6075.
(23) Braun, P. V. *Chem. Mater.* **2014**, *26*, 277.
(24) Galisteo-López, J. F.; Ibisate, M.; Sapienza, R.; Froufe-Pérez, L. S.; Blanco, Á.; López, C. *Adv. Mater.* **2011**, *23*, 30.
(25) Velev, O. D.; Gupta, S. *Adv. Mater.* **2009**, *21*, 1897.
(26) Yang, Q.; Li, M. Z.; Liu, J.; Shen, W. Z.; Ye, C. Q.; Shi, X. D.; Jiang, L.; Song, Y. L. *J. Mater. Chem. A* **2013**, *1*, 541.
(27) Datta, S. S.; Abbaspourrad, A.; Amstad, E.; Fan, J.; Kim, S. H.; Romanowsky, M.; Shum, H. C.; Sun, B. J.; Utada, A. S.; Windbergs, M.; Zhou, S. B.; Weitz, D. A. *Adv. Mater.* **2014**, *26*, 2205.
(28) Shang, L. R.; Cheng, Y.; Wang, J.; Ding, H. B.; Rong, F.; Zhao, Y. J.; Gu, Z. Z. *Lab Chip* **2014**, *14*, 3489.
(29) Shah, R. K.; Shum, H. C.; Rowat, A. C.; Lee, D.; Agresti, J. J.; Utada, A. S.; Chu, L. Y.; Kim, J. W.; Fernandez-Nieves, A.; Martinez, C. J.; Weitz, D. A. *Mater. Today* **2008**, *11*, 18.
(30) Sackmann, E. K.; Fulton, A. L.; Beebe, D. J. *Nature* **2014**, *507*, 181.
(31) Cheng, Y.; Zheng, F. Y.; Lu, J.; Shang, L. R.; Xie, Z. Y.; Zhao, Y. J.; Chen, Y. P.; Gu, Z. Z. *Adv. Mater.* **2014**, *26*, 5184.
(32) Chen, H. S.; Zhao, Y. J.; Li, J.; Guo, M.; Wan, J. D.; Weitz, D. A.; Stone, H. A. *Lab Chip* **2011**, *11*, 2312.
(33) Song, Y.; Chan, Y. K.; Ma, Q. M.; Liu, Z.; Shum, H. C. *ACS Appl. Mater. Interfaces* **2015**, *7*, 13925.
(34) Nge, P. N.; Rogers, C. I.; Woolley, A. T. *Chem. Rev.* **2013**, *113*, 2550.
(35) Zhao, Y. J.; Cheng, Y.; Shang, L. R.; Wang, J.; Xie, Z. Y.; Gu, Z. Z. *Small* **2015**, *11*, 151.
(36) Rossow, T.; Heyman, J. A.; Ehrlicher, A. J.; Langhoff, A.; Weitz, D. A.; Haag, R.; Seiffert, S. *J. Am. Chem. Soc.* **2012**, *134*, 4983.
(37) Liu, W.; Shang, L. R.; Zheng, F. Y.; Lu, J.; Qian, J. L.; Zhao, Y. J.; Gu, Z. Z. *Small* **2014**, *10*, 88.
(38) Lee, S. S.; Kim, B.; Kim, S. K.; Won, J. C.; Kim, Y. H.; Kim, S. H. *Adv. Mater.* **2015**, *27*, 627.
(39) Kim, S. H.; Jeon, S. J.; Yang, S. M. *J. Am. Chem. Soc.* **2008**, *130*, 6040.
(40) Duan, C. H.; Karnik, R.; Lu, M. C.; Majumdar, A. *Proc. Natl. Acad. Sci. U. S. A.* **2012**, *109*, 3688.
(41) Shchukin, D. G.; Skorb, E.; Belova, V.; Möhwald, H. *Adv. Mater.* **2011**, *23*, 1922−1934.
(42) Azouzi, M. E. M.; Ramboz, C.; Lenain, J. F.; Caupin, F. *Nat. Phys.* **2013**, *9*, 38.
(43) Hsu, M. F.; Nikolaides, M. G.; Dinsmore, A. D.; Bausch, A. R.; Gordon, V. D.; Chen, X.; Hutchinson, J. W.; Weitz, D. A.; Marquez, M. *Langmuir* **2005**, *21*, 2963.

DOI: 10.1021/jacs.5b10612
J. Am. Chem. Soc. 2015, 137, 15533−15539